Supplemental Data: Tables 1 - 3; Figures 1 to 5

SAMPLE AND METHODS

The sintered monazite ($LaPO_4$) ceramic used in the present study was prepared according to the protocol described in Picot et al. (2008) and used in (Deschanels et al., 2014). Several Focused Ion Beam (FIB)-foils (12 x 6 x 0.1 μm) were cut perpendicular to the surface of the polycrystalline sample by the *in situ* lift-out technique on a FEI dual-beam microscope (Hélios600i) at the LAAS laboratory in Toulouse, France. The TEM foils were fixed on both sides on the central post of a 3-post Omniprobe Lift-Out 3 mm Grid to increase their stability during the irradiation experiments, as shown in Figure 3. The *in situ* irradiation experiments were performed at room temperature conditions on the JANNuS-Orsay/SCALP platform (Chauvin et al., 2007; Bacri et al., 2017) at the CSNSM, (Univ Paris-Sud and CNRS, Université Paris-Saclay, France), which offers unique capabilities in terms of ions radiation damage studies by coupling two accelerators (ARAMIS and IRMA) with the JANNuS Transmission Electron Microscope (TEM, Tecnai G2 20 Twin). The use of Au^{2+} ions at 1.5 MeV allows the simulation of the nuclear energy loss of the recoil nucleus of an α-decay ($S_{nucl.} \sim 4.5$ keV/nm) without implanting Au atoms in the lamella (range of 215 nm). He^{+} ions at 160 keV simulate the electronic energy loss of the α-particle released in α-decay ($S_{elec.} \sim 0.25$ keV/nm) without implanting He atoms in the lamella (range of 550 nm). Because both particles have a range greater than the thickness of the lamella, their respective fluxes (He-flux/Au-flux = 150) were chosen to simulate the ratio of the damaged volumes of both particles of an α-decay, i.e. the damage volume of the α-particle is around 190 times higher than that of the recoil nucleus. To evaluate the recovery effect of α-particles on the damage state induced by heavy recoil nuclei, three configurations were investigated: the first sequential, and the third simultaneous (Figs. 2-3). All three used the same ions and accelerating energy: 1.5 MeV Au^{2+} ions (ARAMIS accelerator) to induce ballistic damage and 160 keV He^{+} ions (IRMA accelerator) to induce electronic excitations without implanting He atoms in the lamella (Table 1a).

In the first experiment (Fig. 1), Au irradiation up to $2x10^{14}$ Au/cm² (1.13 dpa) is used to fully amorphize the monazite sample (Picot et al., 2008; Deschanels et al., 2014), and ten He irradiation steps are subsequently performed up to a fluence of $5x10^{16}$ He/cm² to evaluate the recovery of the fully amorphized material due to electronic energy loss of He ions (Table 1a). The second experiment (Fig. 2) is similar to the first and aims at evaluating the He-induced recovery of a partially damaged material (0.2 dpa), corresponding to a monazite with a strained lattice (Deschanels et al., 2014), and structurally similar to natural monazite samples (Seydoux-Guillaume et al., 2004). The third experiment (Fig. 3) involve simultaneous irradiation by Au and He ions, up to fluences of $2x10^{14}$ Au/cm² and $3.4x10^{16}$ He/cm², performed in 4 steps. All these experiments were performed without continuous TEM observation to avoid artefacts (e.g. recrystallization; see Supplemental Fig. 3) from the electron beam (Meldrum et al., 1997b; Deschanels et al., 2014). Therefore, Bright-Field images (BF) and Selective Area Electron Diffraction (SAED) were done rapidly after each irradiation step under conditions carefully chosen to avoid any recrystallization of amorphous areas (0.17 nA at x25500 magnification).

Contribution of the electron beam to the recovery process

One of the questions to answer is the contribution of the electron beam to the recovery process observed in the Au+He sequential irradiation of experiment 1 (Supplemental Fig. 4A-B). Despite that the electron beam was switched off during He irradiation, the electron beam could have influenced the recrystallization process during the imaging of the lamella at each step. To test its influence we have performed a sequential irradiation Au + Electron starting from the same amorphized state (Au fluence of $2x10^{14}$Au/cm²) (Exp. 4; Table 1b and 2; Supplemental Fig. 4 C-D). The first nuclei were observed after 25 minutes of electron irradiation at a dose rate of 1.74 GGy/h, so a dose of 0.7 GGy due to the electron beam. In experiment 1, the first nuclei were observed after 667 minutes of irradiation with He ions, during which we estimated an irradiation time with electrons (due to the lamella imaging) of around 45 minutes. At this step, the dose deposited by He ions and electrons are, respectively,

5.22 and 0.27 GGy. Because the electron dose is more than two time lower than the one needed in experiment 4 to generate the first nuclei (with also a lower dose rate), the sole effect of the electron beam cannot explain the recovery process observed in experiment 1. Therefore, the effect of the He irradiation is the main suspected contribution to this phenomenon.

This was also confirmed by the dual beam experiment, during which we also observed a strong effect of He irradiation after the third steps (10^{14}Au/cm² and $1.7x10^{16}$He/cm²) for which the electron beam exposure time was limited to less than 15 minutes (obj. 2, spot size 6) and cannot explain the recovery process observed; and by the experiment 5 (Table 1b; Supplemental Fig. 5) where nuclei were observed inside the entire TEM foil (Fig. 5D) although only a part of the TEM-foil was observed, i.e. irradiated by the electron beam (Fig. 5C-D).

References cited

Bacri, C.-O., Bachelet, C., Baumier, C., Bourçois, J., Delbecq, L., Ledu, D., Pauwels, N., Picard, S., Renouf, S., and Tanguy, C. (2017) SCALP, a platform dedicated to material modifications and characterization under ion beam. Nuclear Instruments and Methods B, 406, 48-52.

Chauvin, N., Henry, S., Flocard, H., Fortuna, F., Kaitasov, O., Pariset, P., Pellegrino, S., Ruault, M.-O., Serruys, Y., and Trocellier, P. (2007) Optics calculations and beam line design for the JANNuS facility in Orsay. Nuclear Instruments and Methods B, 261, 34-39.

Deschanels, X., Seydoux-Guillaume, A.M., Magnin, V., Mesbah, A., Tribet, M., Moloney, M., Serruys, Y., and Peuget, S. (2014) Swelling induced by alpha decay in monazite and zirconolite ceramics: a XRD and TEM comparative study. Journal of Nuclear Materials, 448, 184-194.

Meldrum, A., Boatner, L.A., and Ewing, R.C. (1997b) Electron-irradiation- induced nucleation and growth in amorphous $LaPO_4$, $ScPO_4$, and zircon. Journal of Material Research, 12, 1816-1827.

Picot, V., Deschanels, X., Peuget, S., Glorieux, B., Seydoux-Guillaume, A.M., and Wirth R. (2008) Ion beam radiation effects in monazite. Journal of Nuclear Materials, 381, 290-296.

Seydoux-Guillaume, A.M., Wirth, R., Deutsch, A., and Schärer, U. (2004) On the microstructure of up to 2 Ga old concordant monazites: a X-ray diffraction and transmission electron microscope study. Geochimica et Cosmochimica Acta, 68, 2517-2527.

Supplemental Table 1a. Experimental conditions

#	Exp. 1 - Complete amorphization (Fig.1)		Exp. 2 - Intermediate irradiation (Fig.2)**					Exp. 3 - Dual-beam irradiation (Fig.3)			
Flux (ion/cm²/s)	**Au**	2.0×10^{10}	**Au**	2.0×10^{10}				**Au**	2.0×10^{10}		
	He	3.0×10^{12}	**He**	3.0×10^{12}				**He**	3.0×10^{12}		
Fluence (ion/cm²)	**Au**	4 steps up to 2.0×10^{14}	**First cycle**	**Au**	2 steps up to 2.0×10^{13}	**Second cycle**	**Au**	1 step up to 5.0×10^{13}	**Step1:** 1.0×10^{13} (Au) + 1.7×10^{15} (He)	**Step2:** 5.0×10^{13} (Au) + 7.2×10^{15} (He)	**Step3:** 1.0×10^{14} (Au) + 1.7×10^{16} (He)	**Step4:** 2.0×10^{14} (Au) + 3.4×10^{16} (He)
	He	10 steps up to 5.0×10^{16}		**He**	5 steps up to 1.0×10^{16}		**He**	4 steps up to 5.0×10^{15}				
E_{elec} (keV/cm³)*	4.8×10^{22} (Au)	2.2×10^{24} (He)	**First cycle**	4.8×10^{21} (Au)	4.3×10^{23} (He)	**Second cycle**	1.2×10^{22} (Au)	2.2×10^{23} (He)	**Step1**: 4×10^{21} (Au) + 7.1×10^{22} (He)	**Step2:** 1.2×10^{22} (Au) + 3.1×10^{23} (He)	**Step3:** 2.4×10^{22} (Au) + 7.2×10^{23} (He)	**Step4:** 4.8×10^{22} (Au) + 1.5×10^{24} (He)
E_{nucl} (keV/cm3)*	8.9×10^{22} (Au)	1.5×10^{22} (He)		8.9×10^{21} (Au)	3.0×10^{21} (He)		2.2×10^{22} (Au)	1.5×10^{21} (He)	**Step1:**4.5×10^{21} (Au) + 5.0×10^{20} (He)	**Step2:** 2.2×10^{22} (Au) + 2.2×10^{21} (He)	**Step3:** 4.5×10^{22} (Au) + 5.0×10^{21} (He)	**Step4:** 8.9×10^{22} (Au) + 1.0×10^{22} (He)
E_{elec}/E_{nucl}	21		**First cycle**	36		**Second cycle**	10		15	13	15	15
TEM observation conditions* **	Cond. 3, Obj. 2, α=-41°; β=22.5° Spot size 6, Mag. SA 25.5K (0,17 nA) SAED L=890 mm		Cond. 3, Obj. 2, α=0°; β=22.5°, Spot size 6, Mag. SA 25.5K (0,17 nA); SAED L=890 mm									

All irradiation experiments were performed with 1.5 MeV Au^{2+} ions (ARAMIS) and 160 keV He^{+} ions (IRMA).

*Energy deposited by Au or He by electronical (E_{elec}) or nuclear ($E_{nucl.}$) processes at the end of the experiments. For the third experiment energies are given for each step. $E_{elec.}/E_{nucl.}$ = ($E_{elec.}$ Au + $E_{elec.}$ He)/($E_{nucl.}$ Au + $E_{nucl.}$ He)

** Two irradiation cycles were performed. The first one up to 2.0×10^{13}Au/cm² followed by He irradiation (5 steps up to 1.0×10^{16}He/cm²). The second one up to 5.0×10^{13}Au/cm² followed by He irradiation (4 steps up to 5.0×10^{15}He/cm²).

*** All experiments were performed without continuous TEM observation in order to avoid artefact (e.g. recrystallization) from the electron beam (see Suppl. Fig. 3)

Supplemental Table 1b. Experimental conditions

#	Exp. 4 - Complete amorphization (Suppl. Fig.4C-D)**		Exp. 5 - Electron irradiation (Suppl. Fig.5D-F)***	
Flux (ion/cm²/s)	**Au (1,5 MeV)**	$2.0x10^{10}$	**Au (1,5 MeV)**	$2.5x10^{10}$
	He (1,5 MeV)	$1.0x10^{12}$		
Fluence (ion/cm²)	**Au (1,5 MeV)**	1 step up to $2.0x10^{14}$	**Au (1,5 MeV)**	1 step up to $2.0x10^{14}$
	He (1,5 MeV)	8 steps up to $5.0x10^{16}$		
E_{elec} (keV/cm³)*	$4.8x10^{22}$ (Au)	$2.3x10^{24}$ (He)	$4.8x10^{22}$ (Au)	
E_{nucl} (keV/cm3)*	$8.9x10^{22}$ (Au)	$2.5x10^{21}$ (He)	$8.9x10^{22}$ (Au)	
E_{elec}/E_{nucl}	26			
TEM observation conditions	Cond. 3, Obj. 2, α=-41°; β=22.5° Spot size 6 (0,17 nA), Mag. SA 25.5K SAED L=890 mm		Cond. 3, Obj. 2, α=-41°; β=22.5° Spot size 6 (0,17 nA), Mag. SA 25.5K SAED L=890 mm	

*Energy deposited by Au or He by electronical (E_{elec}) or nuclear ($E_{nucl.}$) processes at the end of the experiments. $E_{elec.}/E_{nucl.}$ = ($E_{elec.}$ Au + $E_{elec.}$ He)/($E_{nucl.}$ Au + $E_{nucl.}$ He)

** Experiment performed without continuous TEM observation in order to avoid artefact (e.g. recrystallization) from the electron beam (see Suppl. Fig.3).

***After amorphization the same area is observed continuously in the TEM in order to follow the effects of the electron beam. The conditions used for this experiment is: Cond. 3, Obj. 2, spot 6, Magnification x25,5K (0,80 nA).

Supplemental Table 2. Conditions for which the first nuclei were observed during the experiments described in Supplemental Figure 4.

Conditions for which the first nuclei were	Exp. 1 (Suppl. Fig. 4A-B)		Exp. 4 (Suppl. Fig. 4C-D)
	He	**Electron** Obj. 2, Spot size 6	**Electron** Obj. 2, Spot size 3
Irradiation time	667 min	45 min	25 min
Dose rate (GGy/h)	0.47	0.36	1.74
Dose (GGy)	5.22	0.27	0.7

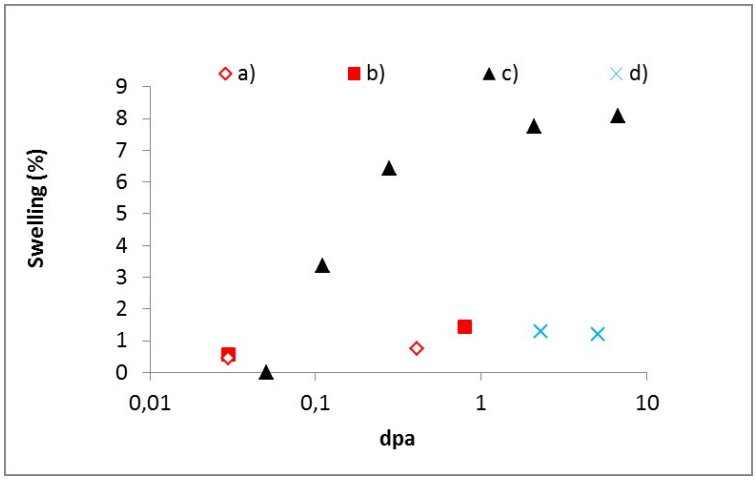

Supplemental Figure 1. Comparison of the swelling of various monazite samples as a function of radiation damage. a) Macroscopic swelling of ^{238}Pu-doped monazite (Deschanels et al., 2014), b) Microscopic swelling of ^{238}Pu-doped monazite (Deschanels et al., 2014), c) Macroscopic swelling of monazite irradiated by multi-energy Au ions (1, 3.5, 7 MeV; Deschanels et al., 2014), d) Microscopic swelling of natural monazites (Seydoux-Guillaume et al., 2004). The displacement per atoms (dpa) was calculated through SRIM-2013. The microscopic swelling was estimated through XRD data, and the macroscopic one by density measurements for ^{238}Pu-doped samples and optical interferometry for externally irradiated samples.

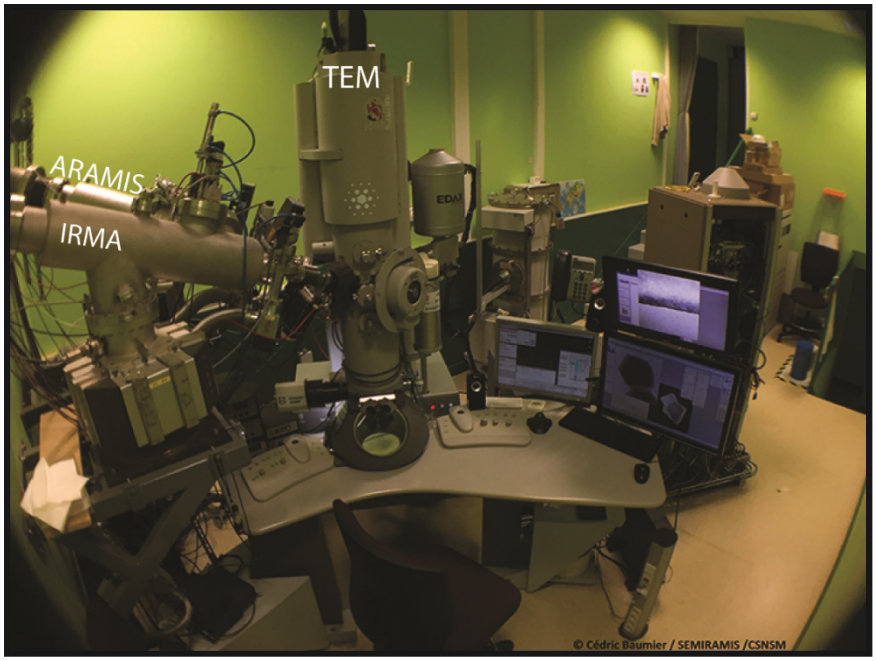

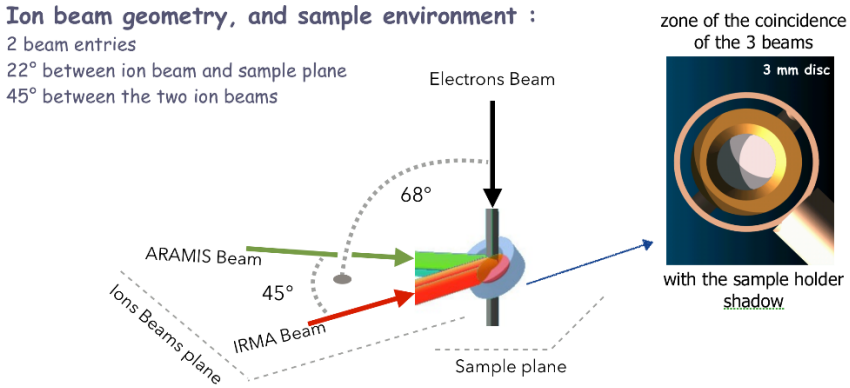

Supplemental Figure 2. Geometry and sample environment of the JANNuS-Orsay/SCALP platform. Photo and design of the accelerators (IRMA and ARAMIS) arriving in the TEM (Chauvin et al., 2007; Bacri et al., 2017). The TEM is a FEI Tecnai G2 20 Twin operating at 200 kV with a LaB_6 gun and equipped with a CCD camera (ES500 with wide angle). The sample holder used for the experiment is a thin double tilt holder that allows tilting of the sample to the appropriate orientation so that the beams arrived on the sample grid as shown on the picture. The geometry of the coincidence between the ions beams and the electron beam allow the use of the shadow effect of the sample holder. More specifically, we are able in one experiment on one sample (a 3 mm diameter grid as on the drawing) to get 3 distinct effects: (1) the largest area (dark grey) see the interaction of the three beams (electron and ions), (2) the white area will see only the electron beam and (3) the light-grey areas will only see the interaction between one of the ion beams and the electron beam from the TEM.

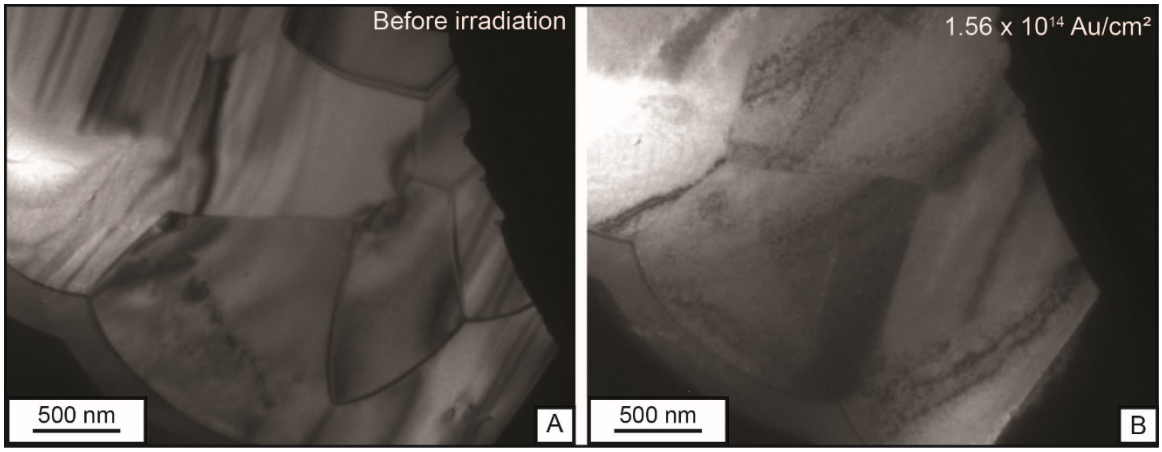

Supplemental Figure 3. Bright-Field Transmission Electron Microscope images (BF-TEM) of the $LaPO_4$ monazite polycrystal TEM foil irradiated with continuous observation on the TEM (i.e. during electron irradiation). A- Part of the TEM foil prepared with focused ion beam (FIB) before irradiation. **B**- Same area as in A *in situ* irradiated up to $1.56x10^{14}$ Au/cm² with continuous electron irradiation. Note that the sample is not amorphous as it should be (compare with Fig. 1B-C) due to the annealing effect of the electron beam. The grain boundaries are still present and only the presence of mottled diffraction contrasts attests for irradiation effects.

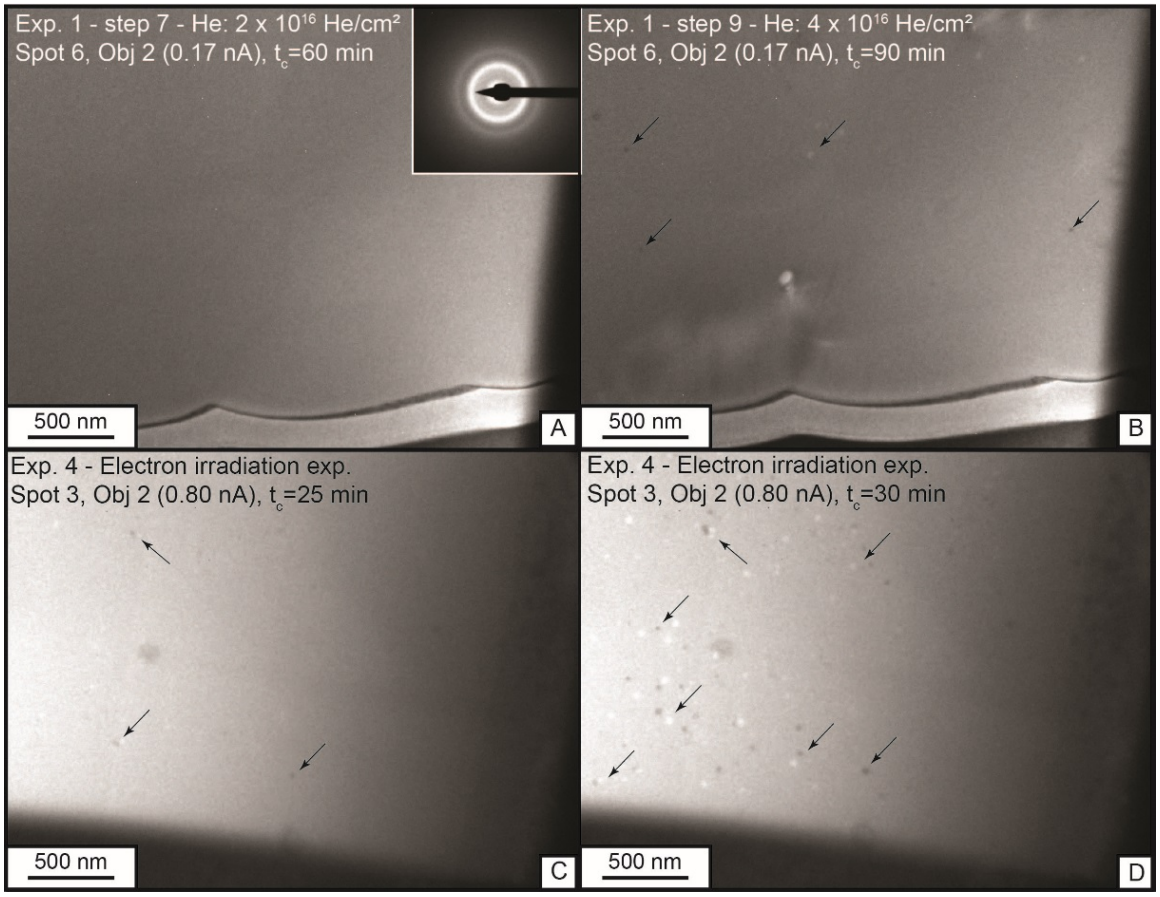

Supplemental Figure 4. Bright-Field Transmission Electron Microscope images (BF-TEM) of two sequences of *in situ* irradiation in $LaPO_4$ monazite polycrystal - Experiment 1 (A-B): sequential Au+He irradiation with electron beam off during irradiation. TEM electron beam was on only during the images acquisition. A- Part of the TEM focused ion beam (FIB) foil after amorphization with Au ions ($2x10^{14}$Au/cm²) and subsequent He irradiation up to $2x10^{16}$ He/cm². No nuclei formed at this step. **B**- Same zone after He irradiation up to $4x10^{16}$ He/cm². Note the presence of nuclei (arrows) that formed in the sample indicating the recrystallization process. The maximum exposure time to electron beam during the sample observation is estimated to be of around 45 minutes. **Experiment 4 (C-D): sequential Au+electron irradiation with electron beam off during Au irradiation (Tables 1b and 2). C-** Part of the TEM focused ion beam (FIB) foil after amorphization with Au ions ($2x10^{14}$Au/cm²) and subsequent electron irradiation with an exposure time of 25 minutes **(C)** and 30 minutes **(D)**. Note that the first nuclei could be detected after 25 minutes of irradiation and that their size and numbers increase rapidly after 30 minutes of irradiation.

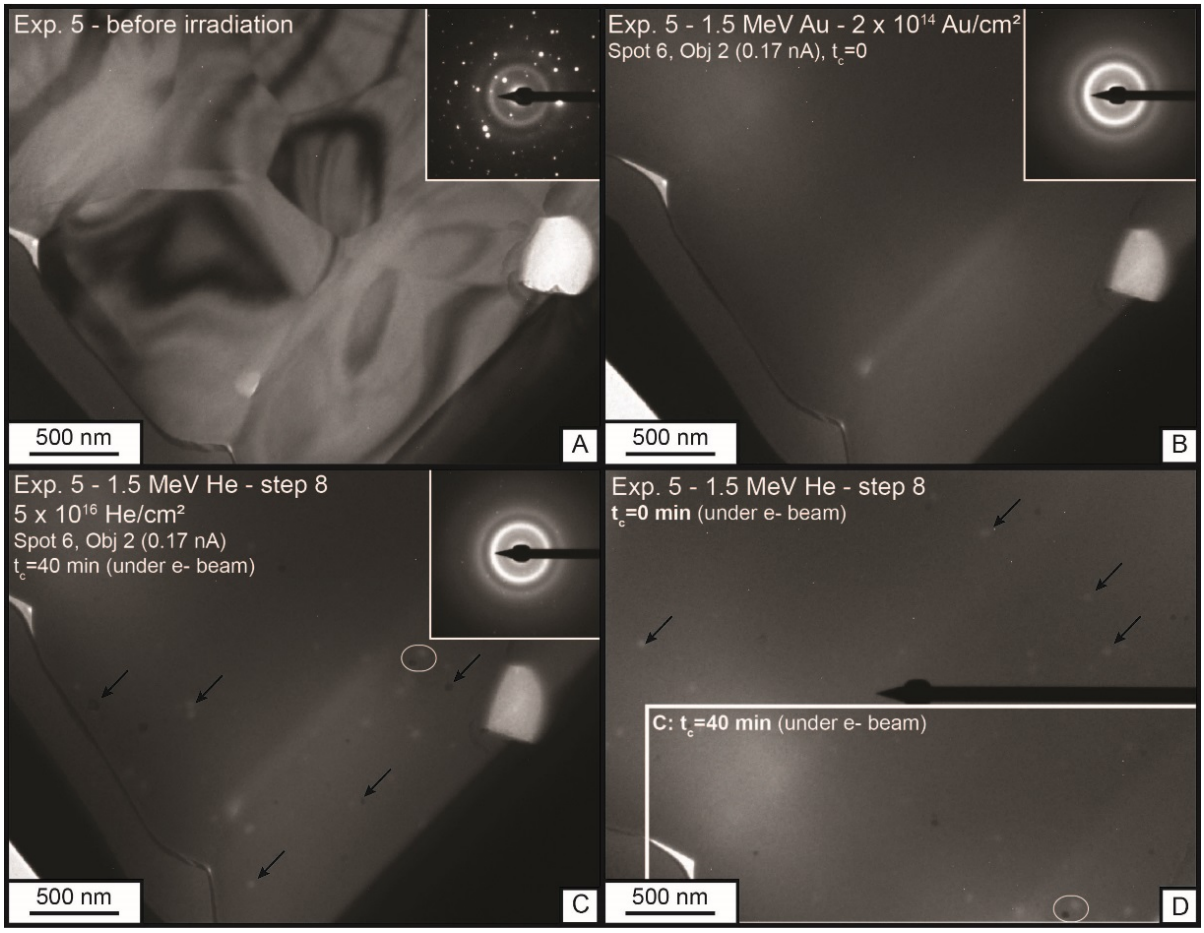

Supplemental Figure 5. Bright-Field Transmission Electron Microscope images (BF-TEM) of a sequence of *in situ* irradiation in $LaPO_4$ monazite polycrystal with Au ions at 1.5 MeV followed by He ions at 1.5 MeV (Experiment 5; Table 1b): A- Part of the TEM focused ion beam (FIB) foil before irradiation. **B**- Same area as in A *in situ* irradiated up to $2x10^{14}$ Au/cm². The sample is completely amorphous as shown by the homogenous contrast on the BF image and the presence of diffuse rings in the selected area electron diffraction (SAED) pattern (inset). **C**- Same area irradiated up to $5x10^{16}$ He/cm². Note the presence of nuclei (arrows) that form in the sample with the corresponding diffraction spots reflecting recrystallization in the SAED pattern. **D**- The lower part of the image corresponds to the same area as in C (see the circle surrounded the same two nuclei on both images). The upper part corresponds to an area never exposed to the electron beam. However, this area also contains nuclei (arrows) whose nucleation can only be due to helium irradiation.